Hindawi
Mathematical Problems in Engineering
Volume 2021, Article ID 6620301, 13 pages
https://doi.org/10.1155/2021/6620301

*Research Article*

# Analysis of Three-Dimensional Vibration Characteristics of Single-Circle Double-Track Subway Tunnel under Moving Load

**Chunquan Dai**,[1,2] **Mengying Yang**,[1,2] **Quanlei Wang**,[1,2] **Tingzhi Yang**,[1,2] **and Kun Jiang**[1,2]

[1]*Shandong University of Science and Technology, Shandong Province Key Laboratory of Civil Engineering & Disaster Prevention and Mitigation, Qingdao 266590, China*
[2]*Shandong University of Science and Technology, Institute of Civil Engineering and Architecture, Qingdao 266590, China*

Correspondence should be addressed to Chunquan Dai; dcqwin@sdust.edu.cn

Received 10 November 2020; Accepted 22 January 2021; Published 3 February 2021

Academic Editor: Jaime Gallardo Alvarado



With the development of urban rail transit, subway lines are becoming more and more denser, the departure time interval is short, and the probability of subway trains meeting is high. The impact of vibration caused by double-line subway meeting on the surrounding environment cannot be ignored. Taking the typical cross-section of a single-circle double-track subway tunnel as an example, a single running scenario and three typical meeting scenarios, namely, 4 s meeting, 6 s meeting, and 8 s meeting scenarios were considered, and a track-tunnel-foundation three-dimensional ABAQUS finite element model was established. The dynamic response of monitoring points at different distances between the center of the track bed and the center line of the track was analyzed. Results showed that due to the consistent load action period, the center acceleration of the track bed increases significantly during the meeting, the main frequency of vibration and the peak value of the 1/3 octave spectrum were increased by about 5 Hz, and the vibration level at the dominant frequency was increased by about 7 dB. The center displacement of the track bed and the peak compressive strain increased significantly under the 4 s meeting and 6 s meeting working scenarios; while the 8 s meeting and 4 s single running scenarios were basically the same, only the action time was doubled. The dynamic response of the 4 working scenarios decreases with the increase of distance, and the attenuation rate gradually decreases and has gradually stabilized within 15–19 m above the vault.

## 1. Introduction

With the acceleration of China's urbanization process, the problem of traffic congestion has become increasingly prominent. As a means of transportation with large volume, high speed, and less ground resources, subways are playing an increasingly important role in daily life and urban development. Large-diameter single-hole double-track subway tunnels are mostly used for long and large tunnels with complex geological scenarios, such as the Nanjing Metro Line 10 cross-river section, Wuhan Metro Line 8 Yangtze River tunnel section, and Qingdao Metro Line 11 Dongshangou tunnel section crossing mountain tunnels. Compared with single-hole single-track tunnels, single-hole double-track tunnels will encounter meeting scenarios, with greater dynamic load and longer acting time. Therefore, it is of great engineering significance to study the vibration characteristics of single-hole double-track tunnel.

Existing studies have conducted beneficial explorations on the vibration characteristics of subway tunnels under moving loads from theoretical calculations, field measurements, and numerical simulations and have achieved certain results. Ren et al. [1] and Lei et al. [2] studied the dynamic response of subway tunnels in saturated soft soil and semi-infinite elastic space caused by subway moving loads by using analytical solutions and 2.5-dimensional finite element methods, respectively. Yuan et al. [3] established a coupling model of saturated soil tunnel and track structure by analytical method and analyzed the dynamic response of the system. Liang [4] used the indirect boundary element method to study the vibration problem of layered foundation induced by subway train vibration. Tang et al. [5]

conducted on-site continuous dynamic monitoring of the tunnel between Jing'an Temple Station and Jiangsu Road Station on Shanghai Metro Line 2 and analyzed the dynamic response of saturated soft clay around the tunnel. He et al. [6] conducted actual measurements on subway train loads and analyzed the main influencing factors of subway train load characteristics. Gao et al. [7] conducted vibration tests on the tunnels of Shanghai Metro Line 1 and used FLAC3D numerical models to analyze the ground vibration response caused by the subway. Lei et al. [8] used ABAQUS to establish a three-dimensional dynamic finite element model and numerically simulated the settlement of soft soil foundation under subway train load. Liu et al. [9] took the first phase of the Tianjin Z2 Metro Line as an example, used ABAQUS to establish a tunnel-soil three-dimensional finite element model, and analyzed the attenuation law of ground vibration intensity.

However, the abovementioned studies only considered the load of the single-track subway, and there are few studies on the dynamic response law caused by the vehicles crossing in the double-track subway tunnel. Hu et al. [10] established a dynamic coupling three-dimensional finite element model of "track-track bed-tunnel-soil" to analyze the dynamic response of the tunnel structure before and after the vehicle intersection of the single-circle double-track tunnel. Xue et al. [11] constructed a dynamic analysis model of the dual-line subway track-tunnel structure-surrounding rock nonlinear coupling system to study the dynamic behavior of the subway tunnel and the surrounding rock under moving loads. However, the abovementioned research only considered the simple working scenarios of a single vehicle or the intersection of two vehicles and did not consider the action time of the vehicle in a given section. In fact, because the initial meeting positions of the up and down trains are not fixed, for a given cross-section, there are multiple combinations of working scenarios for the given cross-section under the load of the double-track train. On this basis, Pan et al. [12] used PLAXIS finite element software to establish a plane finite element model, considering single running scenarios and three typical vehicle crossing scenarios, and analyzed the dynamic response of a single-circle double-track tunnel. However, the model is a plane finite element model, which is relatively simple and cannot reflect the actual engineering situation.

Based on the ABAQUS finite element calculation program, this paper establishes a subway train double-track tunnel-foundation model. From the acceleration, displacement, 1/3 octave spectrum, and fractional frequency vibration level, the dynamic response of different monitoring points under four kinds of passing conditions is analyzed.

## 2. Three-Dimensional Finite Element Model of Single-Hole Double-Track Subway Tunnel

*2.1. Train Operating Scenarios.* Qingdao Metro Line 11 starts at the intersection of Miaoling Road and Shenzhen Road in Laoshan District and ends at Jimo Daqiao Saltworks, with a total length of 58 kilometers. A total of three tunnels are designed across the line, including the Laoshan Tunnel, the Xi'anzi Tunnel, and the Dongshangou Tunnel. The Dongshangou Tunnel is a single-hole double-track tunnel with a total length of 506 meters.

As the up and down trains are running at the same time, multiple combinations of load scenarios may appear at the control section of a single-hole double-track subway tunnel. As shown in Figure 1, considering the situation where subway trains on both sides of the study cross-section appear, the total length of the single-track train is $L$, the speed is $v$, and the time required for the train to completely pass through the section is $T$, and then $T = L/v$; assuming that when the front of the train on one side reaches the position of the research section, the length of the front of the train on the other side that has left the section is $nL$ $(0 \le n \le 1)$, where $n$ is the ratio of the length of the locomotive that has left the section to the total length of the vehicle.

Taking Qingdao Metro Line 11 as an example, the length of the train is 76 m, the running speed is 20 m/s, and then $T = 3.8$ s. As shown in Figure 2, take the front arrival section of the left line train as the reference, and take $n = 0$, 0.5, and 1, respectively. The section length of the right train head is 0, 0.5 $L$, and $L$, respectively. Figure 2(a) shows the position of two trains on the left and right lines passing through the section at the same time, with $T = 3.8$ s. Figure 2(b) shows that after the right line train passes through the section position for 1.9 s, the left line train head just arrives at the section position, and the two trains have a meeting time of 1.9 s in the whole process of passing through the section, with $T = 5.7$ s. Figure 2(c) shows that when the train on the right line completely reaches the section, the head of the train on the left line just reaches the section position, and there is no meeting between the two trains on the section, with $T = 7.6$ s. Define the three working scenarios in Figures 2(a)–2(c) as the working scenarios of "4 s meeting," "6 s meeting," and "8 s meeting".

In addition, Figure 2(d) also shows the typical working condition of only left train passing through the section. Since there is no meeting, with $T = 3.8$ s, the working condition is defined as "4 s single running scenario."

*2.2. Model Size and Material Properties.* When performing finite element analysis, a large part of the efficiency of calculation depends on the size of the mesh of the model. Xue and Zhang [13] showed that the contact pressure distribution on the wheel-rail contact surface is complex and uneven, and the stress on the contact spot can be as high as 1000 MPa, which will bring severe challenges to the calculation convergence. Therefore, in the case of meeting the accuracy, it is very important to choose a reasonable mesh size to reduce the computational workload.

Based on ABAQUS numerical calculation software, a three-dimensional finite element model of track-tunnel-stratum is established, as shown in Figure 3. Figure 3(a) is a schematic diagram of the model grid division, the length of the model along the longitudinal direction of the line is 200 m, the width is 100 m, and the height is 50 m. The tunnel adopts a double-layer lining structure. The track system consists of steel rails, track

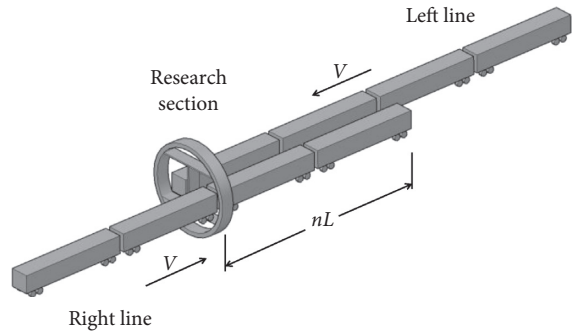


Figure 1: General scenario of train operation in single-circle double-track tunnels.

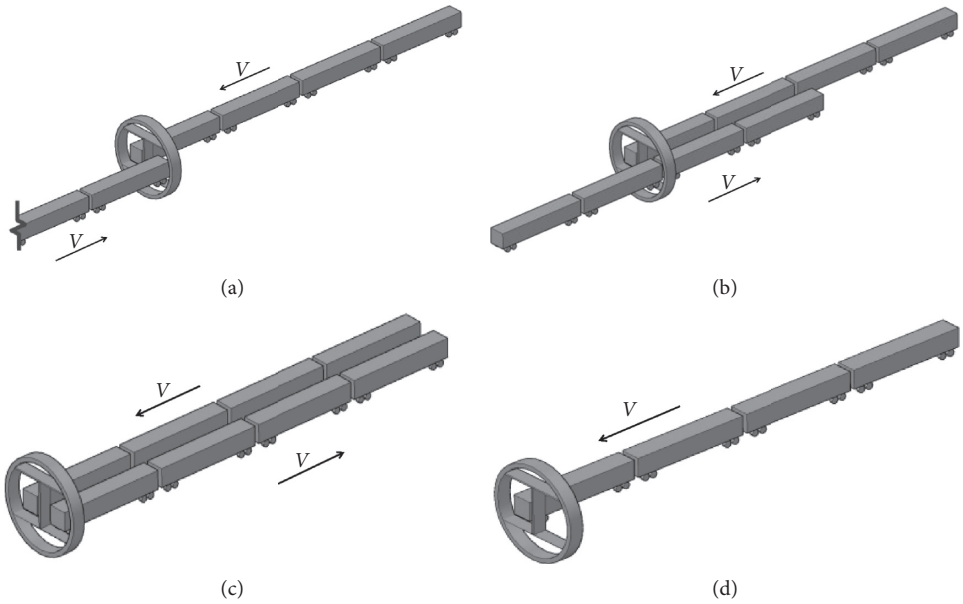


Figure 2: Four typical scenarios. (a) 4 s meeting scenario. (b) 6 s meeting scenario. (c) 8 s meeting scenario. (d) 4 s single running scenario.

slabs, bottom plates, and track beds. The grid division size of the track is set to 0.05 m, and each structural layer of the track-subgrade-foundation system adopts 8-node solid units. The entire model has a total of 259,368 nodes and a total of 240,400 elements, all of which are C3D8R.

As shown in Figure 3(b), the inner diameter of the tunnel is 11.2 m, the outer diameter is 12 m, the inner lining is 0.3 m, the segment lining is 0.5 m, and the middle of the tunnel is the traffic tunnel layer. Two lanes are arranged on the left and right. The distance between the left and right lanes of the traffic lane is 5 m. For the partition wall, the concrete strength grade is C35. The subway rail adopts 60 kg·m$^{-1}$ standard rail with a gauge of 1.435 m. The fasteners are generally arranged at equal intervals with a distance of 650 mm. The connection between the rail and the fastener is spring damper, and the stiffness of the fastener is horizontal and vertical and the longitudinal equivalent stiffness is 37.5, 25, and 37.5 kN·m$^{-1}$, respectively. Below the rail are the track plate, bottom panel, and track bed, with thicknesses of 0.2 m, 0.3 m, and 3.1 m, respectively.

The soil is divided into 3 layers, from top to bottom are filled soil, clay, coarse sand, and granite. According to the structural characteristics, the steel rail and the following structural layers are regarded as infinite homogeneous elastic bodies, followed by the track slab and the bottom layer. The lining structure and the soil body maintain the deformation coordination between the contact surfaces through tie contact. The foundation soil is regarded as an elastic-plastic material, and the model boundary adopts three-dimensional viscoelastic artificial boundary scenarios.

In dynamic calculations, the most commonly used method for the damping coefficient of soil is the Rayleigh damping method. The physical and mechanical parameters of the soil layer of the site are shown in Table 1, and the structural parameters of the track system and tunnel are shown in Table 2.

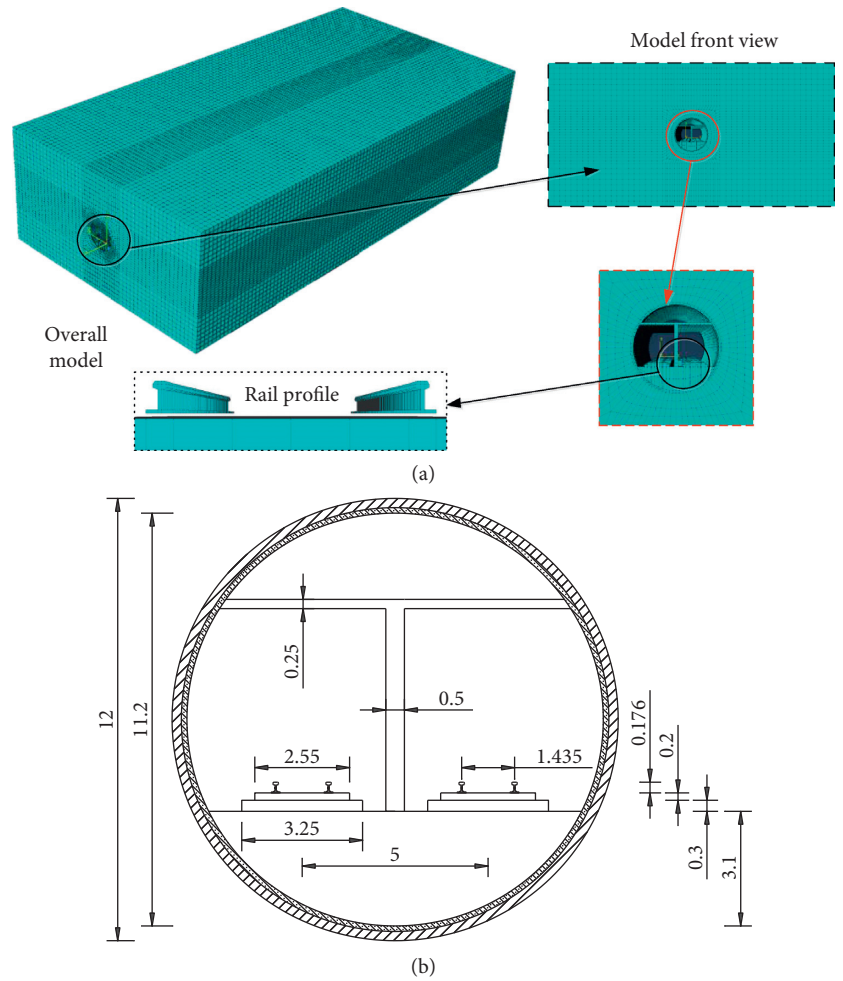


Figure 3: Finite element calculation model. (a) Diagram of model mesh division. (b) Schematic diagram of tunnel structure.

Table 1: Physical and mechanical parameters of soil layer.

| Layer | Thickness (m) | Density (kg·m$^{-3}$) | Compression modulus (MPa) | Poisson's ratio ($\nu$) | Cohesion (kPa) | Internal friction angle (°) | Damping ratio ($\zeta$) | Rayleigh damping ($\alpha$) | Rayleigh damping ($\beta$) |
|---|---|---|---|---|---|---|---|---|---|
| Filling | 4 | 1800 | 5.3 | 0.32 | 9 | 12.5 | 0.08 | 0.2391 | 0.02675 |
| Clay | 12 | 1830 | 6.2 | 0.28 | 35.2 | 25.1 | 0.068 | 0.2033 | 0.00274 |
| Silty | 34 | 1970 | 6.9 | 0.29 | 41 | 18.1 | 0.06 | 0.1794 | 0.02006 |

Table 2: Track system and tunnel structure parameter.

| Name | Thickness (m) | Density (kg·m$^{-3}$) | Elastic modulus (MPa) | Poisson's ratio ($\nu$) | Damping ratio ($\zeta$) | Rayleigh damping ($\alpha$) | Rayleigh damping($\beta$) |
|---|---|---|---|---|---|---|---|
| Track | 0.176 | 7800 | 210 | 0.3 | 0.01 | 0.14488 | 0.00069 |
| Track slab | 0.2 | 2500 | 35.5 | 0.1 | 0.03 | 0.08968 | 0.01003 |
| Floor | 0.3 | 2500 | 30 | 0.1 | 0.03 | 0.08968 | 0.01003 |
| Ballast | 3.1 | 2400 | 28 | 0.1 | 0.03 | 0.08968 | 0.01003 |
| Lining | 0.3 | 2400 | 28 | 0.1 | 0.03 | 0.08968 | 0.01003 |
| Segment | 0.5 | 2400 | 30 | 0.1 | 0.03 | 0.08968 | 0.01003 |

*2.3. Subway Train Load.* The dynamic load of train on the track during subway operation includes three parts: moving dynamic load, fixed action point dynamic load, and moving axle load. This article mainly studies the vibration characteristics of the tunnel and the soil, so the influence caused by the wheel-rail contact irregularity is ignored, and only the vertical load of the train is considered.

The DLOAD train load and the ABAQUS program are combined to realize the train load application. The train is simulated as a series of axle loads. Bian et al. [14] expressed the continuous axle load generated by the train with the following formula:

$$\begin{aligned} P_M &= \sum_{n-1}^{M} f_n(x-ct), \\ f_n(x-ct) &= P_{n1}\delta\left(x-ct+\sum_{n=0}^{n-1}L_n+L_0\right)+P_{n1}\delta\left(x-ct+a_n+\sum_{n=0}^{n-1}L_n+L_0\right)+P_{n2}\delta\left(x-ct+a_n+b_n+\sum_{n=0}^{n-1}L_n+L_0\right) \\ &\quad +P_{n2}\delta\left(x-ct+2a_n+b_n+\sum_{n=0}^{n-1}L_n+L_0\right), \end{aligned} \tag{1}$$

where $P_{n1}$ and $P_{n2}$ represent the axle load of the front and rear wheels of the train, respectively; $L_n$ is the length of each subway; $L_0$ is the distance between the measuring point and the first carriage; $a_n$ and $b_n$ are the distance between the axes; $\delta$ is the Dirac function of the load. In addition, $c$ is the subway speed.

In this paper, Qingdao Metro Line 11 B type train is selected, with a total of 4 marshalling. The length of the subway train is 76 m, and the length of a single section is 19 m. The train has 16 wheel sets, the center distance of bogie is 12.6 m, the fixed wheelbase is 2.5 m, the marshalling weight is 224 t, and the average axle load is 14 t. The schematic diagram of the load model is shown in Figure 4.

For the 4 s meeting working scenario, the moving load of the train is applied simultaneously on the right and the left line of the model. The loads move in opposite directions and meet in the middle of the model to meet the 4 s meeting scenario. For the 6 s meeting working scenario, the train moving load is also applied on the right and left lines, but the load on the right line is applied $T/2$ ahead of time. Similarly, for the 8 s meeting working scenario, the moving load of the train is also applied on the right and left lines, but the load on the right line is applied $T$ earlier, and for the 4 s single running scenario, only the moving train load on the left line at the rear end of the model is applied and analyzed.

*2.4. Boundary Scenarios.* Viscoelastic artificial boundary method can be used to simulate infinite domain with finite model size. It can well reflect the reflection of dynamic load on the model boundary and consider the elastic recovery performance and radiation damping effect outside the truncated boundary.

The finite element model in this paper adopts the viscoelastic static dynamic artificial boundary proposed by Du et al. [15]. In each direction of the boundary node, a unidirectional spring-damping element fixed at one end is applied. The influence of the infinite medium on the near field is simulated by viscous damping energy absorption and spring stiffness recovery. The spring damper parameters of the three-dimensional viscoelastic artificial boundary are as follows:

$$\begin{aligned} \text{Normal } K_l &= \frac{1}{1+A}\frac{\lambda+2G}{r}, \\ C_l &= B\rho c_p, \\ \text{Tangential } K_l &= \frac{1}{1+A}\frac{G}{r}, \\ C_l &= B\rho c_s, \end{aligned} \tag{2}$$

where $\rho$ is the density of the medium, $C_p = \sqrt{(\lambda+2G)/\rho}$ and $C_s = \sqrt{G/\rho}$ are the wave speeds of compression waves and shear waves, respectively; $A$ represents the ratio of the amplitude content of plane waves and scattered waves, reflecting the propagation characteristics of waves on artificial boundaries; $B$ represents the relationship between physical wave velocity and apparent wave velocity. The values of $A$ and $B$ can be obtained through experimental experience. Generally, $A$ is 0.8 and $B$ is 1.1. The length $r$ represents the distance from the geometric center of the near field structure to the boundary line or surface where the artificial boundary point is located. In this paper, the four sides and bottom of the foundation adopt viscoelastic boundaries to simulate wave propagation from finite domain to infinite domain.

*2.5. Monitoring Point Selection.* In order to accurately analyze the dynamic response law of subway vibration to the surrounding soil, a total of 6 monitoring points were selected. The moving load of the subway train is applied by compiling the DLOAD subroutine, and the speed is 20 km/h. The tunnel buried depth and stratum distribution are shown in Figure 5. Six monitoring points $A \sim F$ are selected above the tunnel. Point $A$ is the center point of the track bed, and point F is the monitoring point on the surface directly above

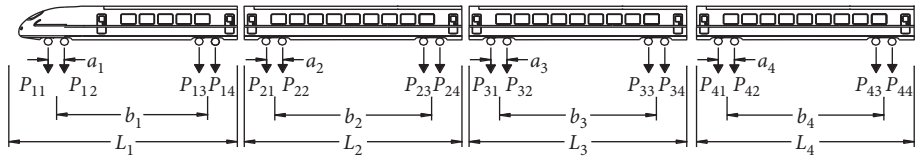


Figure 4: Schematic diagram of the moving load model of subway train.

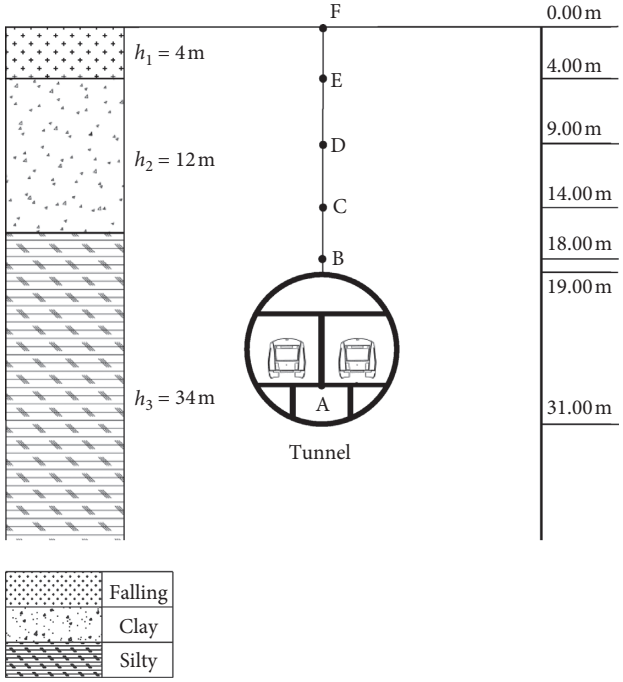


Figure 5: Tunnel and soil distribution.

the track center. The distance between $B \sim F$ and tunnel vault is 1 m, 5 m, 10 m, 15 m, and 19 m, respectively. The abovementioned monitoring points are used to simulate the variation trend of soil dynamic response with depth. Since point $A$ is the center of the track bed and is at the same distance from the left and right lines, the load has the characteristics of symmetrical distribution. In addition, point $A$ is closer to the track, which can better reflect the dynamic response of the tunnel structure caused by subway crossing. Therefore, point $A$ is selected as the key monitoring point, and the dynamic response is mainly discussed.

## 3. Model Validation

In order to check the accuracy of the numerical model, the dynamic response of the tunnel structure was analyzed with reference to the actual test situation. Liu [16] conducted field tests on subway tunnel sections. In the test, the data acquisition application is the INV3060S 24-bit network distributed synchronous acquisition instrument. For vibration acceleration testing, the Lance AS0130 series vibration acceleration sensor is used. Liu [16] conducted field tests on the vertical acceleration of the tunnel wall and compared the results with the numerical model to verify the accuracy of the numerical model.

On this basis, this paper selects the relevant parameters of the numerical model in reference [16]. The model has a horizontal width of 60 meters, a height of 50 meters, and a longitudinal length of 30 meters. The soil layer is divided into two layers, and the tunnel depth is 16 m. The mechanical parameters of the soil layer, tunnel lining, track bed, and other structures in the numerical model are the same as those in the reference. The boundary condition adopts viscoelastic artificial boundary, the unit size of the soil is 0.3–1.2 m, and the unit size is gradually widened when it is far from the vibration source. The speed of the circular tunnel is 60 km/h, and the axle load of the train is 15 $t$, and a three-dimensional model is established. The longitudinal section of the tunnel is selected as the analysis section to analyze the dynamic response of the tunnel structure. The acceleration time history curve of tunnel wall is selected and compared with the measured results in reference [16], as shown in Figure 6.

It can be seen from the comparison of Figure 6 that the acceleration measured value of the tunnel wall of the tunnel structure is basically consistent with the numerical calculation result. It can be seen from the time history curve that the acceleration peaks are similar in size. The tunnel wall acceleration peak calculated by the model is 0.15 m/s$^2$, and the measured acceleration peak is 0.16 m/s$^2$. There are multiple peaks in both the measured and model acceleration curves. Most of the time the acceleration is mainly concentrated at 0.05 m/s$^2$. Comprehensive analysis shows that the numerical model and train load have good similarity and reliability.

## 4. Environmental Vibration Response Analysis

*4.1. Acceleration Spectrum Analysis.* Figure 7 shows the acceleration time history curve at point $A$ of the center of the track bed under different crossing scenarios. It can be seen from the figure that the peak acceleration of 4 s single running scenario is 0.67 m/s$^2$. Due to the consistent load action period of the subway trains, the elastic wave is superimposed and strengthened synchronously, and the peak acceleration of the 4 s meeting working scenario of the passing train is 1.29 m/s$^2$, which is about twice that of the 4 s single running scenario. In the 6 s meeting working scenario, the two trains meet at the cross-section position at 4–6 s, and the dynamic load produces a superimposing effect. Since the two loads have the same period of action, the acceleration peak also increases significantly after the waveform is superimposed. In the 8 s meeting working scenario, the trains on both sides actually pass through the cross-section sequentially, so the acceleration peak is the same as the 4 s single running scenario, but the time is doubled.

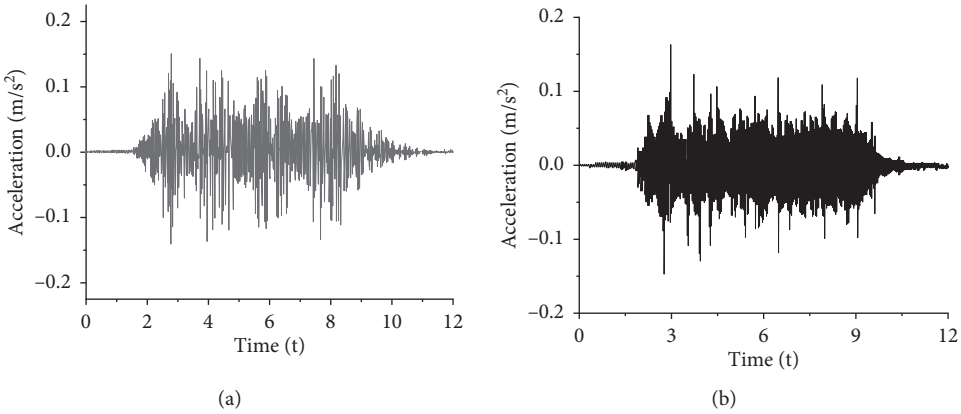


Figure 6: Comparison of acceleration time history curves of tunnel walls. (a) Calculated. (b) Measured.

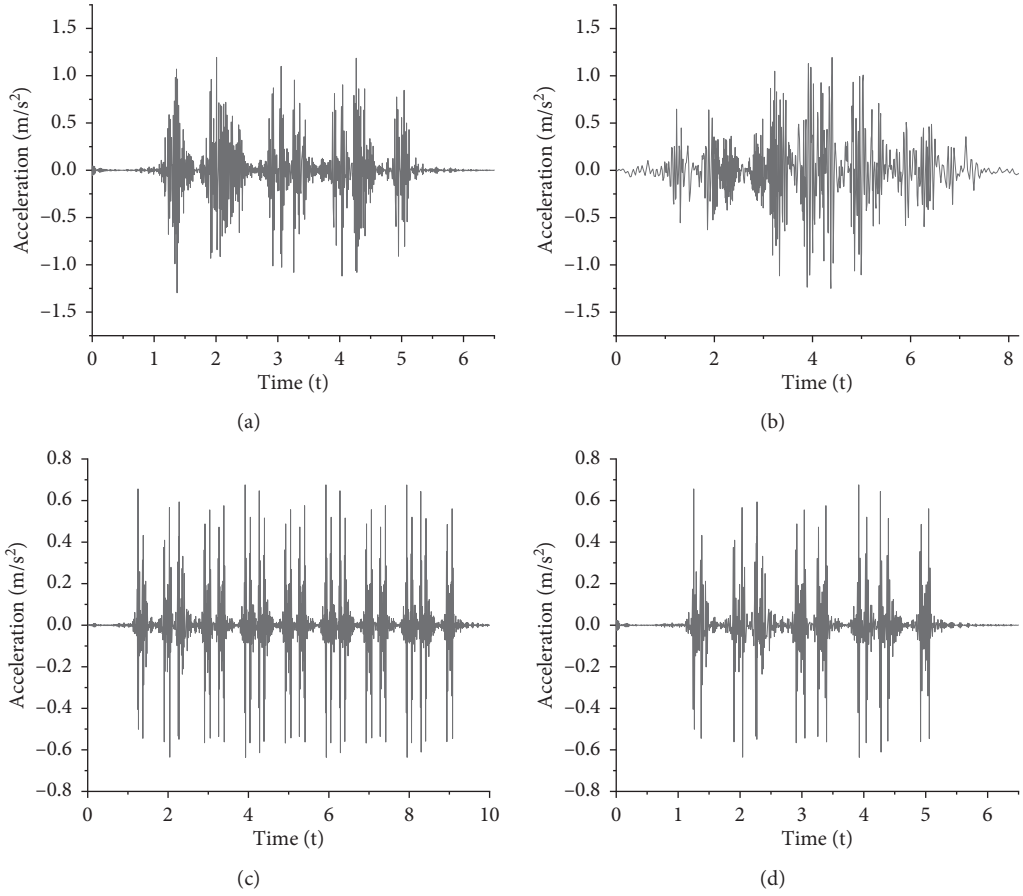


Figure 7: Acceleration time history spectrum of orbit center. (a) 4 s meeting scenario. (b) 6 s meeting scenario. (c) 8 s meeting scenario. (d) 4 s single running scenario.

Figure 8 shows the curve of the acceleration peak value at different distances from the track center line. It can be seen from the figure that within 19 m above the vault, the acceleration peaks under the four working scenarios all show a decay trend with increasing distance, and the decay rate decreases with increasing distance. Point *B*, which is 1 m away from the vault, has the largest acceleration in 4 s meeting working scenario, reaching 0.0448 m/s$^2$, and it also reaches 0.0437 m/s$^2$ in 6 s meeting scenario, which is twice the effect of 4 s single running scenario. At a distance of 19 m from the surface, the acceleration peaks of the four working scenarios are very close, which indicates that the damping effect of the soil makes the elastic wave energy attenuate significantly along the propagation direction.

Figure 9 shows the spectrum curve at point *A* of the center of the track bed under different working scenarios. It

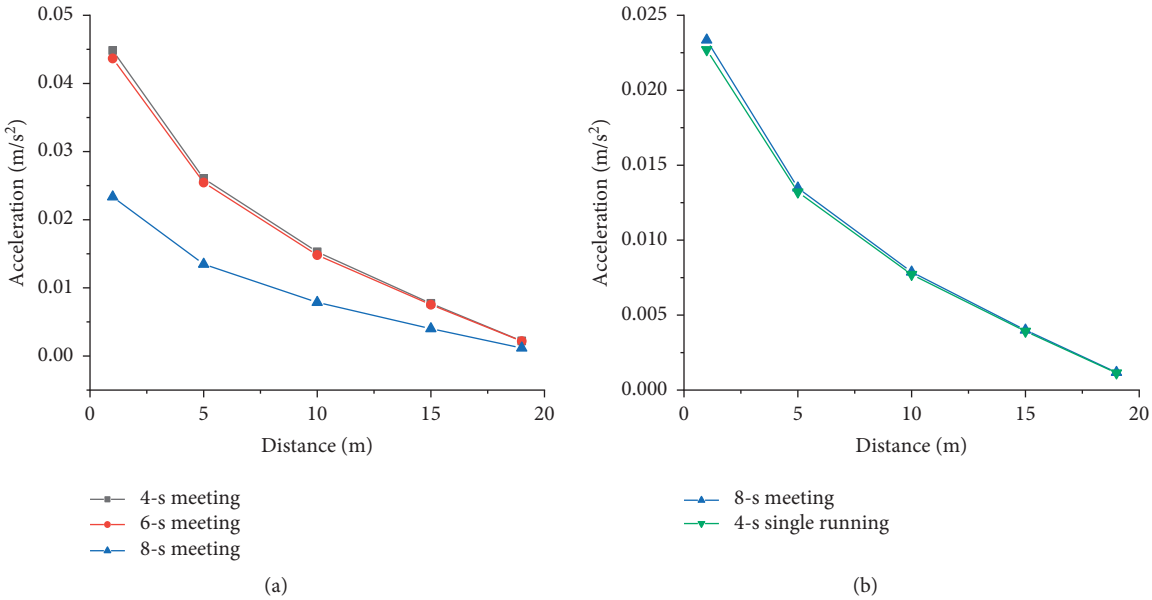


Figure 8: Acceleration decays with distance. (a) Comparison curve of acceleration between 4 s, 6 s, and 8 s meeting scenarios. (b) Comparison curve of acceleration between 8 s meeting and 4 s single running scenarios.

can be seen from the figure that when the vehicle speed is 20 m/s, the center frequency of the track bed in the 4 s single running scenario is mainly controlled by the low frequency, and the main frequency of the track center is within 20 Hz. The main frequency of the center vibration of the track bed is increased in the 4 s meeting and the 6 s meeting working scenarios, and high-frequency components appear. The vertical acceleration amplitude of the vibration in the main frequency band is about 1.9 times and 1.7 times of the single running scenario. The main frequency and corresponding acceleration amplitude of the 8 s meeting working scenario have also been improved. In general, the main frequency of vibration will be transferred to high frequency when subway trains meet.

*4.2. Vibration Level Analysis.* In order to evaluate the environmental vibration caused by subway operation, the spectrum curve is transformed into 1/3 octave spectrum. Then, the vibration level is calculated according to equation (3) proposed by Esveld [17]:

$$L_a = 20\lg\left(\frac{a_1}{a_2}\right), \tag{3}$$

where $L_a$ is the vibration level, $a_1$ is the effective value of vertical acceleration in each 1/3 octave band (m/s$^2$), and $a_2$ is the standard acceleration value ($10^{-6}$ m/s$^2$).

The 1/3 octave spectrum can be realized in two ways: One is to band-pass filtering the sampled signal according to different center frequency definitions in the entire frequency range, calculate the root mean square value (RMS) of the filtered data, and obtain the power spectrum value corresponding to each center frequency. Another method is to perform fast Fourier transform on the sampled signal first to calculate the power spectrum or amplitude spectrum and then use the power spectrum or amplitude spectrum data to calculate the average value within the bandwidth of each center frequency.

According to the definition of RMS value and discretization, we can get

$$\mathrm{RMS} = \sqrt{\frac{1}{T}\int_0^T x^2(t)\mathrm{d}t} = \sqrt{\frac{1}{N\Delta}\sum_{n=0}^{N-1} x^2(n\Delta)\cdot\Delta} = \sqrt{\frac{1}{N}\sum_{n=0}^{N-1} x^2(n)}, \tag{4}$$

where $\Delta$ is the sampling interval, $x(t)$ is the continuous signal time course, and $x(n)$ is the discrete signal time course. Figure 10 shows the 1/3 octave spectrum and the average value of the divided frequency vibration level at point $A$ of the track bed center under different working scenarios. It can be seen from the figure that the peaks of the 1/3 octave spectrum of the 4 s single running and 8 s meeting working scenarios are both 16 Hz, and the vertical acceleration peaks are 0.12 m/s$^2$ and 0.11 m/s$^2$, respectively. The peak value of the 1/3 octave spectrum in the 4 s meeting and 6 s meeting working scenarios is around 20 Hz, and the peak vertical acceleration is increased to 0.24 m/s$^2$ and 0.21 m/s$^2$.

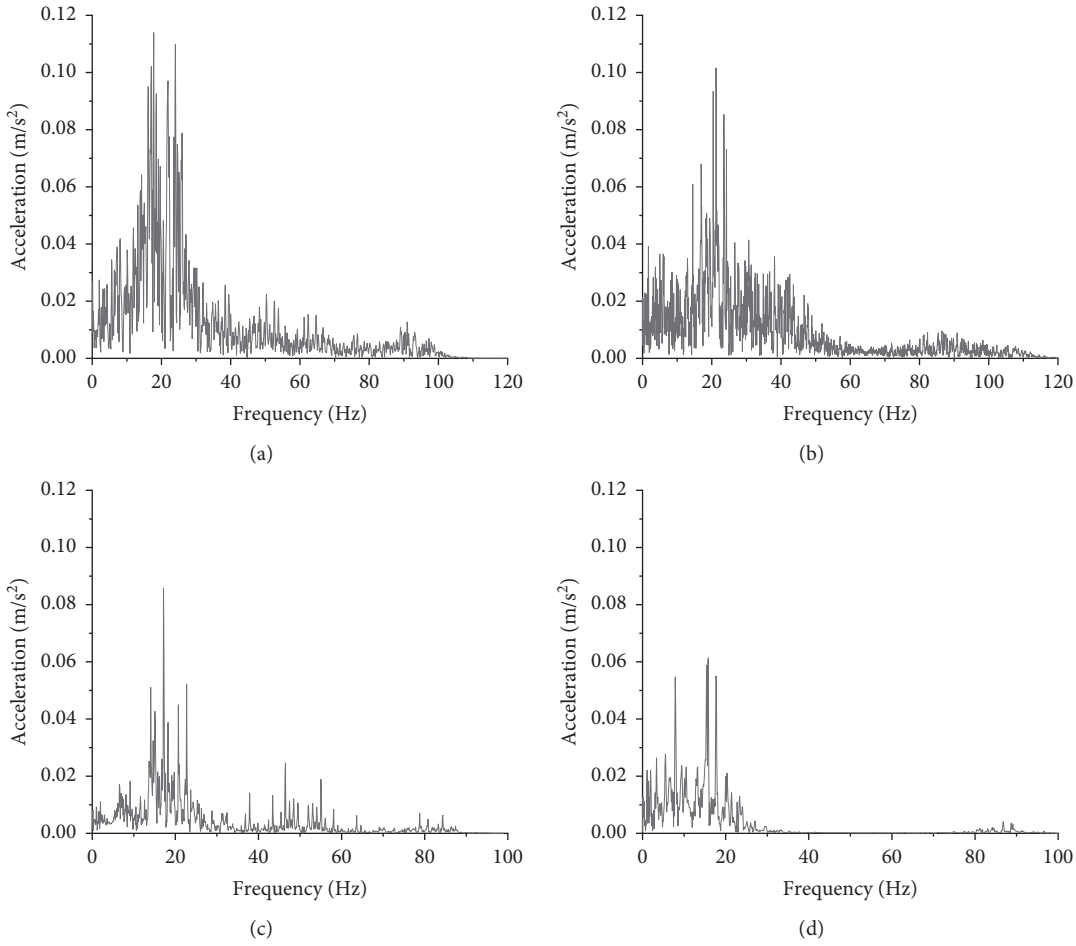


Figure 9: Spectrum curve of orbit center. (a) 4 s meeting scenario. (b) 6 s meeting scenario. (c) 8 s meeting scenario. (d) 4 s single running scenario.

It shows that the dominant frequency of the track bed vibration has increased, which is consistent with the results of the spectrum analysis.

It can be seen from the average value of the frequency division vibration level that the vibration levels at the dominant frequency for the 4 s meeting and 6 s meeting working scenarios are, respectively, 105 dB and 104 dB, which are about 7 dB higher than the 4 s single running scenario. In addition, although the vibration level of the 8 s meeting working scenario is not significantly higher than the 4 s single running scenario at the dominant frequency, the vibration level of the other frequency bands is significantly higher than that of single running scenario.

According to China's Standard of Environmental Vibration in Urban Area (GB10070-88), the standard limit of vertical vibration level in general commercial and residential mixed areas of cities is 75 dB during the day and 72 dB at night. The environmental vibration caused by subway operation exceeding the vibration level limit can affect human health, and the vibration level will be significantly increased when subway trains meet. Therefore, it is of great significance to accurately evaluate the vibration response value caused by subway operation.

*4.3. Displacement Time History Analysis.* Figure 11 plots the time history curve of vertical displacement at point A of the track bed center under different working scenarios. It can be seen in the figure that the center displacement of the track bed increases cyclically during the passage of the train wheel/rail, and the wheel/rail starts to rebound slowly after passing. The peak value of the vertical displacement in the 4 s single running scenario is 0.59 mm. Due to the simultaneous superposition of train loads, the peak value of the vertical displacement in the 4 s meeting working scenario is 1.28 mm, which is twice that of the single vehicle.

In the 6 s meeting working scenario, the vertical displacement is also superimposed during the train rendezvous time, and the peak value of the vertical displacement is 1.7 times that of the 4 s single running scenario. In addition, because the trains on both sides pass through the cross-section in sequence during the 8 s meeting working scenario, the peak vertical displacement is 0.6 mm, which is basically the same as the 4 s single running scenario. Only the number of vertical displacement fluctuations caused by the wheel and rail is doubled.

Figure 12 shows the maximum displacement trend of the monitoring points at different depths on the track center

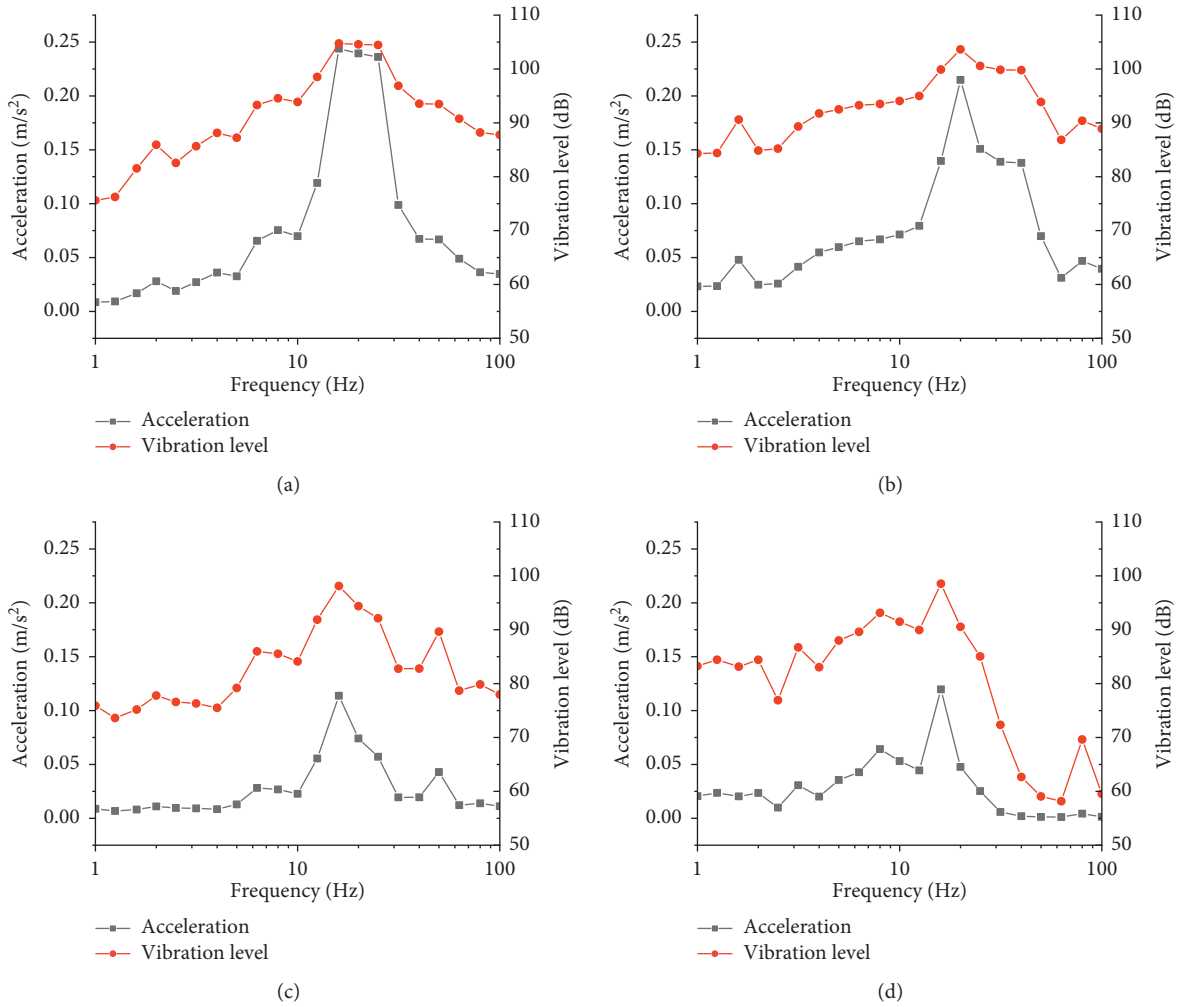


Figure 10: The 1/3 octave spectrum and the average value of the divided frequency vibration level at point *A* of the track bed. (a) 4 s meeting scenario. (b) 6 s meeting scenario. (c) 8 s meeting scenario. (d) 4 s single running scenario.

line. It can be seen from the figure that the maximum displacement of the soil shows a decreasing trend with the increase of distance, but the decreasing rate gradually decreases. In the range of 10–19 m, the maximum vertical displacement gradually stabilizes. The maximum vertical displacement at different depths is observed for the 4 s meeting scenario, followed by the 6 s meeting, 8 s meeting, and 4 s single running scenarios. The maximum vertical displacement of the abovementioned 4 working scenarios is 1.046, 0.926, 0.554, and 0.545 mm, and the minimum displacement is 0.436, 0.386, 0.236, and 0.227 mm.

Figure 13 plots the time history curve of the horizontal displacement of point *A* of the center of the track bed under different working scenarios. It can be seen from the figure that the horizontal displacement peak value in the 4 s meeting working scenario is 0.051 mm, which is about 1.8 times that of the 4 s single running scenario. Therefore, the load is superimposed in the 6 s meeting working scenario, and the horizontal displacement of point A increases in 3~5 s. After superimposition, the horizontal displacement of point A increases to 1.5 times that of the single running scenario. In addition, the peak horizontal displacement of point A in the 8 s meeting working scenario is basically the same as that of the 4 s single scenario; only the displacement fluctuation time is doubled.

*4.4. Dynamic Strain Analysis.* When subway vehicles are running in the tunnel (multiple intersection conditions), the moving load will produce the coupling vibration between the vehicle and the tunnel structure, which will lead to the dynamic strain of the track. The dynamic strain caused by vibration affects the fatigue life and service life of tunnel structure. Therefore, the analysis of dynamic strain caused by moving load has very important theoretical significance and practical value.

Figure 14 plots the dynamic strain time history curve of point *A* in four kinds of meeting working scenarios. It can be seen from the figure that the compressive strain peak appears in the center of the track bed under the action of the train load, and when the wheel set is not acting, the compressive strain rapidly decreases and approaches to zero. The maximum compressive strain at point *A* reaches 11.9 $\mu$m under

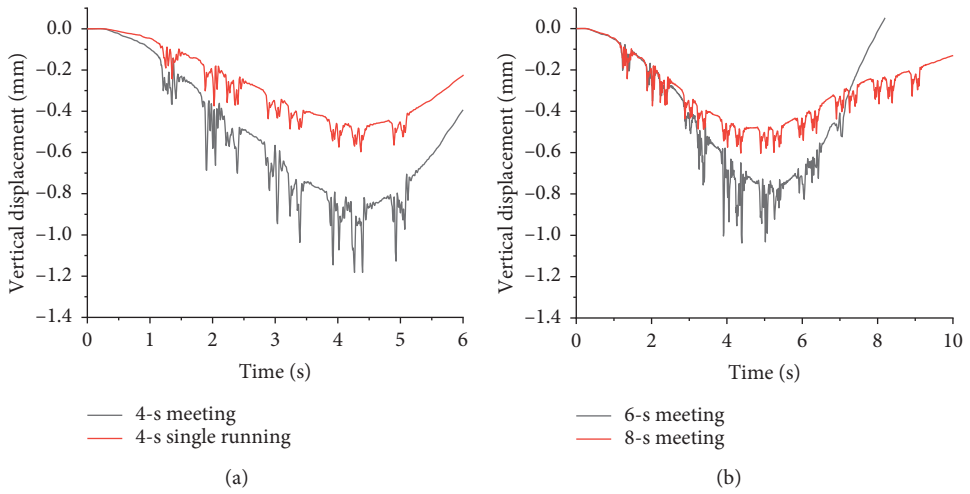


Figure 11: Time history curve of vertical displacement of track center. (a) Comparison curve of vertical displacement time between 4 s meeting and 4 s single running scenarios. (b) Comparison curve of vertical displacement time between 6 s and 8 s meeting scenarios.

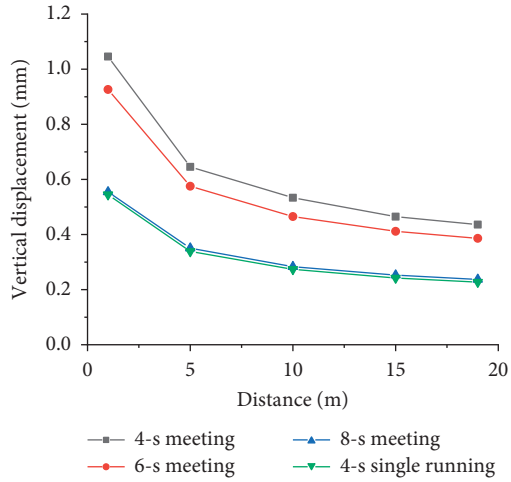


Figure 12: Vertical displacement attenuates with distance.

4 s single running scenario and 23.5 $\mu$m under 4 s meeting scenario, which is approximately twice that of 4 s single running scenario. The maximum compressive strain at 6 s meeting scenario also reaches 22.1 $\mu$m, which is approximately 1.8 times that of a single vehicle.

Figure 15 shows the attenuation trend of dynamic strain at different foundation depths on the track center line. It can be seen from the figure that the closer to the train load position, the greater the dynamic strain of the soil. The strain at point $B$, which is closest to the tunnel vault, reaches the maximum strain at 381 $\mu$m in 4 s meeting working scenario. Within 19 m above the vault, the maximum dynamic strain of the soil decreases with the increase of the distance. For different distance points under different working scenarios, the maximum strain of the soil is observed for the 4 s meeting scenario, followed by the 6 s meeting, 8 s meeting, and 4 s single running scenarios, and the dynamic strain of the soil under 8 s working scenario is very close to the 4 s single running scenario due to the action time being doubled.

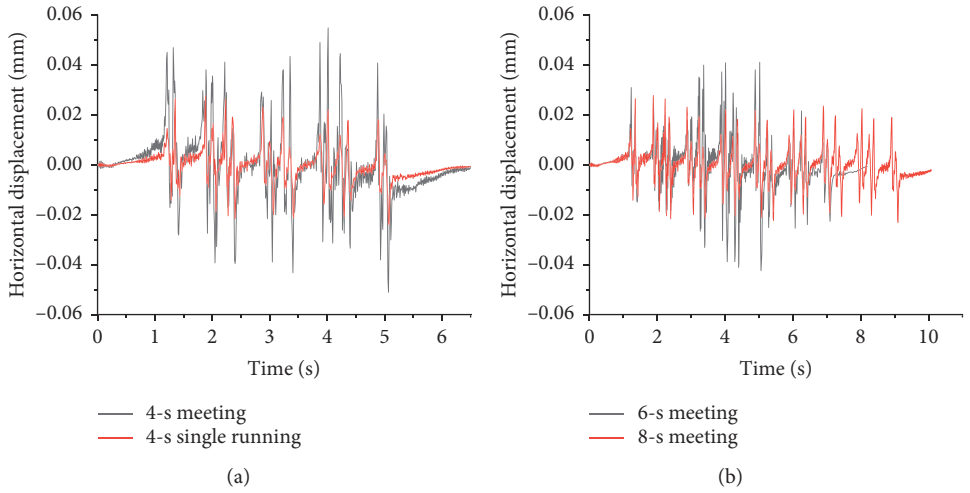


Figure 13: Time history curve of horizontal displacement of track center. (a) Comparison curve of horizontal displacement time between 4 s meeting and 4 s single running scenarios. (b) Comparison curve of horizontal displacement time between 6 s and 8 s meeting scenarios.

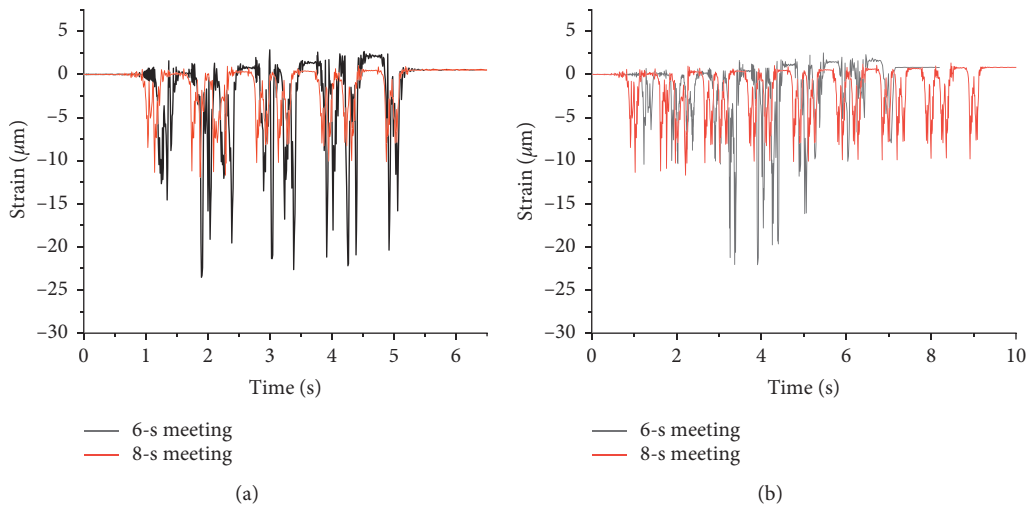


Figure 14: Strain time history spectrum of point A (a) Comparison spectrum of strain time history between 4 s meeting and 4 s single running scenarios. (b) Comparison spectrum of strain time history between 6 s and 8 s meeting scenarios.

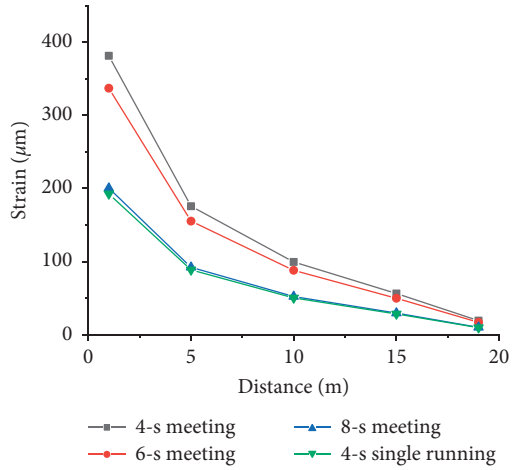


Figure 15: Vertical strain attenuates with distance.

## 5. Conclusions

This paper takes the engineering construction of Dongshangou tunnel section of Qingdao Metro Line 11 as the background to study the vibration response of subway tunnels. Based on the ABAQUS finite element calculation program, a metro train double-track tunnel-foundation model is established. The dynamic response and the monitoring points at different distances from the track center line under four driving scenarios are analyzed.

The main conclusions are as follows:

(1) Due to the same load action period during the meeting, the center acceleration of the track bed in the 4 s and 6 s meeting working scenarios increased significantly, the main frequency of vibration and the peak value of the 1/3 octave spectrum increased by about 5 Hz, and the vibration level at the dominant frequency increased by about 7 dB. The environmental vibration generated by subway operation exceeding the limit will affect human health, and the subway train will significantly increase the vibration level.

(2) The vertical displacement, horizontal displacement, and peak compressive strain peaks of the track bed center in the 4 s and 6 s meeting driving scenarios increased significantly, while the 8 s meeting and 4 s single running scenarios are basically the same, only the action time is doubled. Considering the maximum vertical displacement of each depth position under various working scenarios, the maximum displacement is observed for the 4 s meeting scenario, followed by the 8 s meeting, 6 s meeting, and 4 s single running scenarios.

(3) Under different working scenarios, the dynamic response of the monitoring points on the track center line decreases with the increase of distance, and the decay rate gradually decreases. The dynamic response is gradually stable in the range of 15–19 m above the vault.

## Data Availability

The data from references [14, 15] used to support the findings of this study are available from the corresponding author upon request. Other data used to support the findings of this study are included within the article.

## Conflicts of Interest

The authors declare that they have no conflicts of interest.

## References

[1] X. Ren, Y. Tang, Y. Xu, Y. Wang, X. Zhang, and S. Liu, "Study on dynamic response of saturated soft clay under the subway vibration loading I: instantaneous dynamic response," *Environmental Earth Sciences*, vol. 64, no. 7, pp. 1875–1883, 2011.

[2] L. Xiaoyan, X. U. Bin, and X. U. Manqing, "Analysis on the dynamic response of metro tunnel under moving load in semi-infinite elastic space by scaled boundary finite element method in frequency-wave domain," *China Railway Science*, vol. 38, no. 1, pp. 77–85, 2017.

[3] Z. Yuan, Y. Cai, and C. Zeng, "Dynamic response of track system and underground railway tunnel saturated soil subjected to moving train loads," *Yanshilixue Yu Gongcheng Xuebao/Chinese Journal of Rock Mechanics and Engineering*, vol. 34, no. 7, pp. 1470–1479, 2015.

[4] J. Liang, B. Zhang, and B. Zhenning, "Effects of site dynamic characteristics on ground vibration induced," *Journal of Earthquake Engineering and Engineering Vibratio*, vol. 35, no. 1, pp. 94–104, 2015.

[5] Y. Q. Tang, Z. D. Cui, X. Zhang et al., "Dynamic response and pore pressure model of the saturated soft clay around the tunnel under vibration loading of Shanghai subway," *Engineering Geology*, vol. 98, no. 3-4, pp. 126–132, 2008.

[6] W. He and W. Xie, "Field measurement of the subway train loading in a car depot," *Journal of Vibration and Shock*, vol. 35, no. 8, pp. 132–137, 2016.

[7] G. Gao, L. Zhu, W. Li et al., "Vibration test and analysis at the people's square of Shanghai, metro line 1," *China Earthquake Engineering Journal*, vol. 36, no. 3, pp. 429–433, 2014.

[8] L. Hua-Yang, Z. Lei, and X. U. Ying-Gang, "Numerical simulation of settlement of soft soil foundation under fast metro train loads," *Chinese Journal of Geotechnical Engineering*, vol. 41, no. S1, pp. 45–48, 2019.

[9] Y. Liu, B. Zhenning, Y. Gao et al., "Influences of metro operation on ground vibration along Tianjin Z2 line," *Chinese Journal of Geotechnical Engineering*, vol. 41, no. S1, pp. 193–196, 2019.

[10] B. Hu, X. Jin, C. Zhan et al., "Numerical simulation of the nonstop crossing of opposite subways in a single bore tunnel," *Journal of Vibration and Shock*, vol. 34, no. 24, pp. 32–39, 2015.

[11] F. Xue and J. Zhang, "True three dimensional dynamic analysis of subway tunnel structure and surrounding soil under moving loads," *Journal of the China Railway Society*, vol. 39, no. 6, pp. 133–140, 2017.

[12] B. Pan, W. Zhang, J. Cao et al., "Dynamic responses of soils around a one-hole double-track tunnel with the metro train meeting," *Shock and Vibration*, vol. 39, 2020.

[13] F. C. Xue and J. M. Zhang, "Spatial distribution of vibration accelerations in coupled rail-embankment-foundation system on high-speed railway under moving loads," *Yantu Gongcheng Xuebao/Chinese Journal of Geotechnical Engineering*, vol. 36, no. 12, pp. 2179–1883, 2187.

[14] X. Bian and Y. Chen, "Dynamic analyses of track and ground coupled system with high-speed train loads," *Chinese Journal of The Oretieal and APPlied Meehanies*, vol. 37, no. 4, pp. 477–484, 2005.

[15] X. Du, Mi Zhao, and J. Wang, "A stress artificial boundary in fea for near-field wave probled," *Chinese Journal of The Oretieal and APPlied Meehanies*, vol. 38, no. 1, pp. 49–56, 2006.

[16] Z. Liu, *Study on Dynamic Response of Metro Tunnel under Train Loads*, Beijing Jiaotong University, Beijing, China, 2017.

[17] C. Esveld, *Modern Railway Track*, MRT-Productions, Zaltbommel, Netherlands, 1989.